STATISTICAL COUPLING BETWEEN TIME POINT-PROCESSES

Samuel Kubler, Jean-Christophe Olivo-Marin, Thibault Lagache

⋆ Institut Pasteur, Université de Paris, CNRS UMR 3691, BioImage Analysis Unit
F-75015 Paris, France.
Corresponding Author: samuel.kubler@pasteur.fr

ABSTRACT

The observation of physical phenomena often goes through the recording of discrete time series of events, that can be represented with marked point processes. The robust estimation of the correlation between two point processes can, therefore, unveil physical mechanisms underlying the observed phenomena. However, the robust estimation of correlation between two, or more, point-processes is hindered by the signal noise (leading to false and missing point detections), the important density of points, and possible time-shift between coupled points. We propose a statistical framework that uses hypothesis testing to estimate coupling between time point-processes. Using simulations, we show that our framework accurately estimates the coupling between two time point-processes even for noisy signal (with false point detections), for high density of points and in the presence of a time shift between coupled points. By applying our statistical framework to the recordings of neuron population activity in mouse visual cortex, we measure the functional coupling between individual neurons, and cluster neurons into functional ensembles.

Index Terms— Time point-processes - Ripley's K function - Statistical coupling - Neuronal spikes - Functional connectivity

1. INTRODUCTION

In many fields, the observation of physical events can only be done through discrete time series of events. This is the case, for example, of volcanic eruptions [1] and earthquakes [2] in geology, molecules arrival and departures form specific processes sites in cellular biology (e.g. endocytosis and pathogen entry [3], and neuronal activity through the firing of action potentials from individual neurons [4] which the study case of the experimental part of our article. The statistical characterization of relations (coupling) between two (or more) time series of events can unveil important mechanisms that underly the observed processes. For example, the observation of the sequential arrival of molecules at endocytic sites with fluorescence microscopy helped to unravel the mechanisms of cell entry [3]. Another example is given by the observation of the firing of individual neurons within a population that provides information on neuronal communication and coding [5].

Observed time series of events can often be modeled as marked point processes [6], with the point being the time location of an event and the mark its attributes (e.g. intensity, color, duration...). Therefore, the characterization of the correlation between different time series of events reduces to the estimation of the coupling between time point-processes. In the case of neuronal activity studies, the two main methods used to estimate the coupling between point-processes are either based on the estimation of underlying firing rates (i.e. the intensity of associated point-processes) [7] and the analysis of the correlation between estimated intensities, or coupling estimation is directly performed with colocalization analysis between discrete time point-processes [4]. While the methods using the estimation of firing rates are more robust to the missing and false detections of single point events, they depend on the robust estimation of firing rates and are not well-suited for detecting the synchronization of single point events. On the other hand, the colocalization methods are sensitive to false and missed point detections. Moreover, high point density can lead to fortuitous point colocalization and overestimation of processes' coupling, whereas time shifts between coupled points can lead to coupling underestimation.

To tackle these technical issues in colocalization analysis, we developed a statistical method to robustly evaluate the coupling between time point-processes, even in the presence of a time-shift between individual coupled points. Our method uses the multi-distance Ripley's K function [8] to measure the time-shifted accumulation of points from one time point-process relatively to the other. It corresponds to an adaptation of state-of-the-art statistics of point-processes to 1-dimensional temporal case of spiking events. This method has been developed to account for false inferred spike detections and potential time-shifts that results from spike deconvolution methods in calcium imaging [14]. As our method is based on statistical characterization of the Ripley's K function and hypothesis testing, it is robust to noise (false point detections) and remains accurate even for high point density. We assess the robustness of our method with synthetic simulations, and show that it outperforms state-of-the-art colocalization metrics. Finally, we use our method to compute the functional relations within a population of neurons in the visual cortex of mice, from their individual spiking activity.

2. METHOD

2.1. Measuring the coupling between time point-processes with the Ripley's K function

Ripley's K function introduced by Brian Ripley in the 70's [8] remains the gold-standard to measure the coupling between spatial point processes.

The idea of our temporal adaptation is to measure the coupling between two time point-processes $s_1 = [t_1, \dots, t_{n_1}]$ and $s_2 = [t'_1, ..., t'_{n_2}]$ by creating a regular mesh grid whose topology is dependent on s_1 point locations in time and by comparing the effective distribution of s_2 points falling in each mesh to the distribution expected under a random distribution assumption through a statistical hypothesis rejection test. Thus, the Ripley's vector $\mathbf{G}_N = [G_0, \dots, G_i, \dots G_{N-1}]$ embeds a 1-dimensional mathematical mesh grid implementation composed by an ensemble of N fixed size rings of radius $[r_i, r_{i+1}]$ centered around s_1 points. Thus, Ripley's function just corresponds to a statistical effective counter

of s_2 points that fall into rings around s_1 objects with a boundary corrective term w which corrects for the potential underestimation of neighbors to points that are close to the starting- and ending-points of the time study period. This correction is inspired by the 2-dimensional corrective term used by Ripley in [8].

$$G_i = \frac{|\Omega|}{n_1 n_2} \sum_{t_k \in s_1} \sum_{t'_l \in s_2} \mathbb{1}_{\{r_i \leq |t_k - t'_l| \leq r_{i+1}\}} w(t_k, t'_l) \quad (1)$$

$$\text{with} \quad w(t_k, t'_l) = 1 + \mathbb{1}_{\{|t_k - t'_l| > |t_k - \delta\Omega(t_k)|\}} \quad (2)$$

where $|\Omega|$ is the length of the time period over which the two time point-processes are observed, $\mathbb{1}$ is an indicator function such that $\mathbb{1}_{\{A\}} = 1$ if A is True, 0 otherwise. $\delta\Omega$ is the coordinate of the closest boundary of the study domain *ie* $\delta\Omega(t_k) = 0$ if $t_k \leq |\Omega|/2, \Omega$ otherwise.

To detect a significant coupling between time series (point-processes) s_1 and s_2, we design an hypothesis testing approach. We compare how far is the effective Ripley's function counter in the rings regarding the number of points expected under a null hypothesis H_0 of Complete Spatial Randmness where points are located according to an homogeneous Poisson distribution for s_2 point-process. Analytical mean and standard deviation parameters are derived by calculating intersection of 1-dimensional volumes corresponding to the overlapping of rings. Under H_0, Ripley's K function tends to a normal distribution [9] in accordance with the central limit theorem. Thus, the distribution of $\mathbf{G} = [G_i]_{i=0..N-1}$ is fully characterized by its mean $M_N = [\mathbb{E}\{G_i\} = \mu_i]_{i=0..N-1}$ and its standard deviation $\Sigma_N = [\mathbb{E}\{G_i^2\} - \mu_i^2 = \sigma_i^2]_{i=0..N-1}$. Using the CSR hypothesis for s_2 time points and the boundary correction (Eq. 2), we compute that

$$\mu_i = \frac{1}{n_1} \sum_{t_k \in s_1} \int_{y \in \Omega} \mathbb{1}_{\{r_i \leq |t_k - y| \leq r_{i+1}\}} \left(1 + \mathbb{1}_{\{|t_k - y| > |t_k - \delta\Omega|\}}\right) dy \quad (3)$$

and

$$\sigma_i^2 = \frac{|\Omega|}{n_1^2 n_2} \sum_{t_k \in s_1} \left(I_{21}(t_k, r_i, r_{i+1}) + \sum_{t_j \in s_1, t_j \neq t_k} I_{22}(t_k, t_j, r_i, r_{i+1}) \right) \quad (4)$$

with

$$I_{21}(t_k, r_i, r_{i+1}) = \frac{-\mu_i^2}{|\Omega|} + \int_{y \in \Omega} \mathbb{1}_{\{r_i \leq |t_k - y| \leq r_{i+1}\}} \left(1 + 3 \times \mathbb{1}_{\{|t_k - y| > |t_k - \delta\Omega|\}}\right) dy$$

$$I_{22}(t_k, t_l, r_i, r_{i+1}) \approx -\frac{\mu_i}{|\Omega|} + \mathbb{1}_{\{|t_k - \delta\Omega| > r_{i+1}\}} \mathbb{1}_{\{|t_l - \delta\Omega| > r_{i+1}\}} \times \int_{y \in \Omega} \mathbb{1}_{\{r_i \leq |t_k - y| \leq r_{i+1}\}} \mathbb{1}_{\{r_i \leq |t_l - y| \leq r_{i+1}\}} dy$$

The size and number of the rings provide a maximum duration beyond which colocalization can no longer be detected and a temporal resolution to distinguish two close interactions.

2.2. Statistical test of time point-processes' coupling

To build a statistical test of time point-processes' coupling, we introduce the reduced statistics

$$\tilde{\mathbf{G}} = \mathbf{A}^{-1} \frac{\mathbf{G} - M_N}{\Sigma_N} \quad (5)$$

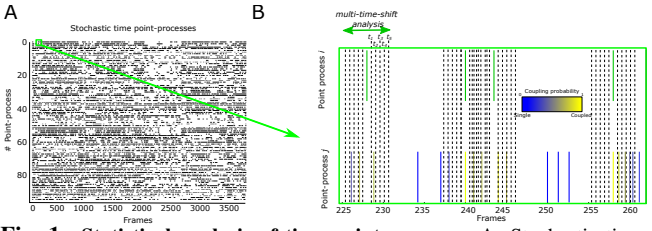

Fig. 1: Statistical analysis of time point-processes A- Stochastic time-point processes (e.g. rasterplot of individual neurons' spiking). **B-** Multi-time-shift analysis of the coupling between two time point-processes. Depending on the accumulation of points from one point-process around the other for different time-shifts, a coupling probability is assigned to each pair of time points.

with $\mathbf{A}$ a correction matrix for ring's overlapping [10]. Under the null hypothesis of s_2 randomness, $\tilde{\mathbf{G}}$ is a standard normal vector (*i.e.* each of its component $\tilde{G}_i \sim \mathcal{N}(0,1)$. Therefore, a significantly high value of a vector component $\tilde{G}_i$ would indicate an accumulation of coupled points around reference points corresponding to a positive coupling (while a low value would indicate a depletion of s_2 points corresponding to a negative coupling).

Similarly to the statistical test introduced for spatial point-processes [10], we use the maximum component of reduced Ripley vector $\tilde{G}_{\max} = \sup_{0 \leq i \leq N-1} \tilde{G}_i$ to test if there is at least one ring $[r_i; r_{i+1}]$ where s_2 time points accumulate significantly. To compute the $p-value$ associated with the observed maximum component $\tilde{G}_{\max}$, we compute that, $\forall x > 0$,

$$\begin{aligned} \Pr\{\tilde{G}_{\max} \geq x\} &= 1 - \Pr\{\forall i \in [1..N-1], \tilde{G}_i < x\} \\ &= 1 - (\Pr\{\mathcal{N}(0,1) < x\})^N = 1 - \text{cdf}^N(x), \end{aligned}$$

where cdf(x) is the cumulative density function of the standard normal law. Finally we obtain the $p-value$

$$\text{p-value} = 1 - \text{cdf}^N(\tilde{G}_{\max}) \quad (6)$$

2.3. Quantitative characterization of time point-processes' coupling

To further characterize the putative coupling between two time point-processes, we determine the components of Ripley's reduced vector $\tilde{\mathbf{G}}$ that are significantly high by using the universal threshold $T(N) = \sqrt{2\log(N)}$ [11], which is widely used in image processing to determine the significant component of a signal corrupted with standard white noise. Thus, $\tilde{G}_i > T(N)$ indicates that there is a significant accumulation of s_2 points at a time shift comprised between r_i and r_{i+1} from s_1 points. This allows the detection of coupling between two time point-processes at different distances and not only the detection of points co-occurence at the same time. Hence, our framework can handle coupling estimation with time shifts and varying delays. Finally, we convert the reduced Ripley vector components into a coupling probability between all the points (t_k, t_l) of time point-processes s_1 and s_2

$$P(t_k, t_l) = \sum_{i=0}^{N-1} \mathbb{1}_{\{r_i \leq |t_k - t_l| < r_{i+1}\}} \frac{\sigma_i \tilde{G}_i \mathbb{1}_{\{\tilde{G}_i > T(N)\}}}{G_i} \quad (7)$$

and extract a global coupling metric on the entire time series

$$GC(s_1, s_2) = \frac{1}{n_1} \sum_{t_k \in s_1} \frac{1}{n_l} \sum_{\substack{t_l \in s_2 \\ P(t_k, t_l) \neq 0}} P(t_k, t_l) \quad (8)$$

where n_l is the number of t_l coupled points in s_2, i.e. such that their coupling probability with t_k in s_1 is strictly positive.

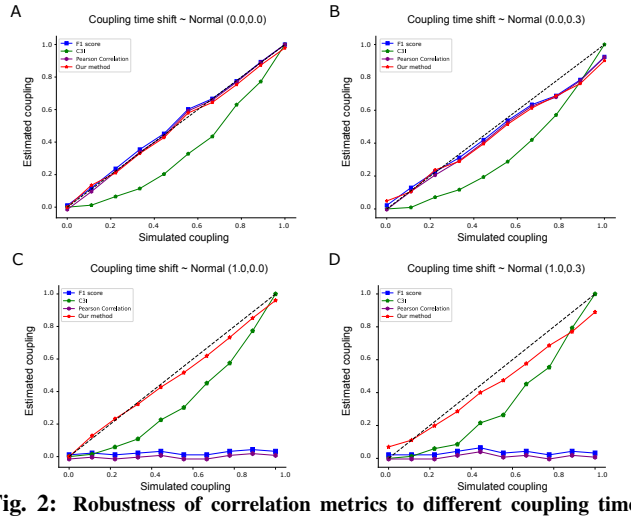

Fig. 2: Robustness of correlation metrics to different coupling time shifts. Our statistical method (red) is compared with standard correlation metrics (Pearson correlation coefficient (purple), F1 score (blue) and C3I (green)) for increasing simulated coupling level and different time shifts (**A-** $t_{shift} \sim \mathcal{N}(\mu_s = 0, \sigma_s = 0)$, **B-** $t_{shift} \sim \mathcal{N}(0, 0.3)$, **C-** $t_{shift} \sim \mathcal{N}(1, 0)$, and **D-** $t_{shift} \sim \mathcal{N}(1, 0.3)$.)

3. RESULTS

3.1. Synthetic simulations

To validate our proposed statistical framework we use simulations where the coupling characteristics between time point-processes are known, and we compare the results of our method to standard measures of signals' correlation.

3.1.1. Robustness to variations of coupling level and time shift

Using simulations of time point-processes with varying coupling level and time shifts, we compare the accuracy of our statistical method with standard correlation metrics (see Appendix for details): **1)** the Pearson correlation coefficient, **2)** F1 score and **3)** the Cluster Core Index (C3I) [12]. To simulate coupled time point-processes with effective coupling level p_c, we first generate a reference homogeneous Poisson point-process s_1, with $n \sim 30$ points over Ω, with length $|\Omega| = 3700$. Then, a proportion $p_c n$ of point process s_2 are coupled to random s_1 points with a time shift $t_{shift} \sim \mathcal{N}(\mu_s, \sigma_s)$, the other $n(1 - p_c)$ points of s_2 being randomly distributed (homogeneous Poisson process over Ω). Finally, to simulate a video acquisition in biological imaging, we discretize the time period $\Omega = \{\Omega_t\}_{1 \leq t \leq T}$, where each Ω_t is a time step with length $\Delta t = 1$.
For increasing simulated levels of coupling and several time shifts ($(\mu_s, \sigma_s) = (0, 0), (1, 0), (0, 0.3)$, and $(1, 0.3)$, we compare our statistical method with other standard methods (Figure 2). For $\mu_s = 0$, i.e. when most coupled time points are co-occurring in same time steps Ω_t, all methods provide a correct estimation of the effective coupling between time point-processes. We highlight that the non-linear, convex shape of C3I curve is due to the used index of correlation [12]. However, when the mean time shift increases to $\mu_s = 1$, our statistical framework and C3I outperform classical correlation coefficients that are not well-equipped for time-shifted coupled point-processes. We conclude that our framework can handle coupling with or without time-shifts between coupled points and correctly estimates the simulated level of coupling.

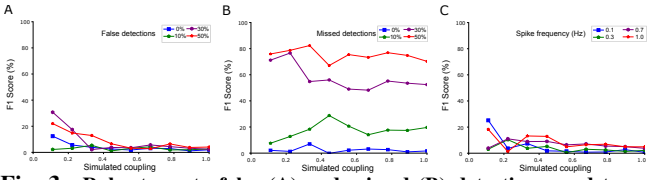

Fig. 3: Robustness to false (A) and missed (B) detections, and to an increased intensity of the time point-process (C).

3.1.2. Robustness to false and missed detections

A common issue when dealing with point-processes is the presence of false and missed detections in time point series. These artefacts are due to the presence of noise in the acquired biological signal. For example, when analyzing the spiking activity of individual neurons with calcium imaging, noise in calcium intensity traces and imperfections in deconvolution algorithms used for extracting neuron discrete spikes (time points) lead to false and missed detections (see section 3.2). In Figure 3, we measure the robustness of our method to increased levels of false and missed detections. We plot the F1 score of the proportion of couples estimated with our method. For any simulated level of false detections (0%, 10%, 30% and 50 %), our method estimates an accurate number of points' couples ($> 80\%$ of couples are recovered). Conversely, our method is much more sensitive to missed detections. Indeed, an increased number of missed detections reduces the number of observable couples. Typically, for a percentage $0 \leq p \leq 1$ of missed points in processes s_1 and s_2, the expected proportion of missed couples will be equal to $1 - p^2$. Finally, we also test the sensitivity of our method to the intensity λ_0 of underlying point-processes. Indeed, an increased intensity (i.e. overall number of points over the observed period $\sim \lambda_0 |\Omega|$), can lead to an increased number of points' couples due to chance. We observe that, actually, our statistical method is very robust to an increased intensity of underlying point processes from $\lambda_0 = 0.1$ Hz to 1 Hz.
From previous simulations, we conclude that our method outperforms other standard correlation methods when there is a time-shift between the coupled points of the two time point-processes, i.e. when coupled points are not necessarily co-occurring in the same time steps. Moreover, we assessed the robustness of our method when false detections (i.e. random points) are added to the original coupled time point-processes, as well as when the intensity of processes is overall increased. The only sensitive parameter is the level of missing points that leads to an expected decreased of detected points' couples.

3.2. Functional coupling between individual neurons

We apply our method to measure the functional coupling between individual neurons from their monitored spiking activity. We use the online dataset from [13], corresponding to two-photon imaging of neuron activity in mouse visual cortex (File M1d1AS in the dataset). From calcium fluorescence traces, the exact spiking times can be obtained using spike inference techniques with variable accuracy and robustness [14]. A representative rasterplot of neuron spiking activity obtained with the constrained FOOPSI deconvolution algorithm [15] is shown in Figure 1-A ($|\Omega| = 5$ minutes, image acquisition rate $= 12.3$ Hz). We measure the coupling between individual neurons using the coupling index (eq. 8) (Figure 4-A). Size of used Ripley's vector (eq. 2) is equal to $N = 4$, with identical time-shifts $r_{i+1} - r_i = 1$ frame (~ 80 ms) for $i = 0..3$. Proportions of coupled spikes for the different time shifts are respectively equal to $[65\%, 13\%, 12\%, 10\%]$, meaning that $2/3$ of the coupled

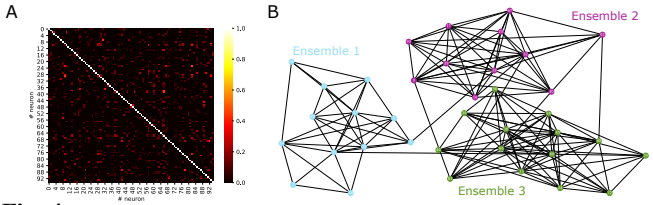

Fig. 4: Analyzing functional coupling between individual neurons in mouse visual cortex. A- Coupling index (eq. 8) between individual neurons computed from their extracted spiking activity (rasterplot). **B-** Network representation and Louvain clustering of neuronal ensembles.

spike times are co-occuring in the same time step Ω_t, while $1/3$ are time-shifted by more than one frame. These latter, time-shifted coupled spikes are completely missed by standard correlation techniques. Using the coupling information between individual neurons, we represent neurons' couples with an undirected network graph, with edges corresponding to strictly positive coupling indexes (Figure 4-B). We identify neuronal ensembles with a Louvain clustering algorithm [16] which maximizes graph modularity, and obtain 3 neuronal ensembles (with $n \geq 10$ neurons), in agreement with [13].
We conclude that our statistical framework allows the robust estimation of functional coupling between individual neurons from the calcium imaging of their spiking activity. Contrary to standard correlation metrics, it allows the estimation of points' coupling even in the presence of time-shifts, and does not require any thresholding of correlation coefficients for the network representation and clustering of neuronal connectivity.

4. CONCLUSION

We have proposed a statistical method for estimating the coupling between time point-processes that use the multi-distance Ripley's K function and hypothesis-testing framework. Our method is able to accurately estimate the coupling between time-shifted correlated point processes, and is robust to high intensity of point processes and false detections. The unique ability of our framework to compute the coupling between time-shifted point-processes is used to quantify the functional coupling between individual neurons imaged with fluorescent calcium indicators in mouse visual cortex [13].

5. APPENDIX

Pearson correlation coefficient For a discretized time period $\Omega = \{\Omega_t\}_{1\leq t\leq T}$, we introduce the indicator functions $\delta_t(s_k) = \mathbf{1}\{\exists t_l \in s_k | t_l \in \Omega_t\}$ for each time-process $\{s_k\}_{k=1,2}$ that determines whether at least one point of each time point-process falls into the time step Ω_t. The Pearson correlation coefficient is then given by

$$r(s_1, s_2) = \frac{\sum_{1\leq t\leq T} \delta_t(s_1)\delta_t(s_2) - T\bar{s_1}\bar{s_2}}{\sqrt{\sum_{1\leq t\leq T} \delta_t(s_1) - T\bar{s_1}^2}\sqrt{\sum_{1\leq t\leq T} \delta_t(s_2) - T\bar{s_2}^2}},$$

with $\bar{s_k} = T^{-1}\sum_{1\leq t\leq T} \delta_t(s_k)$.

F1 score
To compute the F1 score between time point-processes s_1 and s_2, we set a tolerance for point-matching ($tol = 2$ frames) and define *true positive (TP)* as $TP = \sum_{1\leq t\leq T} \delta_t(s_1)\delta_{t\pm tol}(s_2)$ with $\delta_{t\pm tol}(s_2) = \mathbf{1}\left\{\exists t_l \in s_2 | t_l \in \bigcup_{t-tol\leq j\leq t+tol}\{\Omega_j\}\right\}$. *False positive (FP)* and *false negative (FN)* are respectively given by $FP = \sum_{1\leq t\leq T} \delta_t(s_2)(1 - \delta_{t\pm tol}(s_1))$ and $FN = \sum_{1\leq t\leq T} \delta_t(s_1)(1 - \delta_{t\pm tol}(s_2))$. Finally F1 score is equal to

$$F1 = \frac{2\times TP}{2\times TP + (FP + FN)}.$$

6. COMPLIANCE WITH ETHICAL STANDARDS

This is a numerical simulation study for which no ethical approval was required.

7. ACKNOWLEDGMENTS

No funding was received for conducting this study. The authors have no relevant financial or non-financial interests to disclose.

8. REFERENCES

[1] Yvonne Dzierma and Heidi Wehrmann, "Eruption time series statistically examined: Probabilities of future eruptions at villarrica and llaima volcanoes, southern volcanic zone, chile," *Journal of Volcanology and Geothermal Research*, vol. 193, no. 1-2, pp. 82–92, 2010.

[2] Yosihiko Ogata, "Seismicity analysis through point-process modeling: A review," *Seismicity patterns, their statistical significance and physical meaning*, pp. 471–507, 1999.

[3] Cyril Basquin, Michaël Trichet, Helena Vihinen, Valérie Malardé, Thibault Lagache, Léa Ripoll, Eija Jokitalo, Jean-Christophe Olivo-Marin, Alexis Gautreau, and Nathalie Sauvonnet, "Membrane protrusion powers clathrin-independent endocytosis of interleukin-2 receptor," *The EMBO journal*, vol. 34, no. 16, pp. 2147–2161, 2015.

[4] Donald H Perkel, George L Gerstein, and George P Moore, "Neuronal spike trains and stochastic point processes: Ii. simultaneous spike trains," *Biophysical journal*, vol. 7, no. 4, pp. 419–440, 1967.

[5] Luis Carrillo-Reid, Shuting Han, Weijian Yang, Alejandro Akrouh, and Rafael Yuste, "Controlling visually guided behavior by holographic recalling of cortical ensembles," *Cell*, vol. 178, no. 2, pp. 447–457, 2019.

[6] Xavier Descombes and Josiane Zerubia, "Marked point process in image analysis," *IEEE Signal Processing Magazine*, vol. 19, no. 5, pp. 77–84, 2002.

[7] Jean-François Coeurjolly, "Median-based estimation of the intensity of a spatial point process," *Annals of the Institute of Statistical Mathematics*, vol. 69, no. 2, pp. 303–331, 2017.

[8] B. D. Ripley, "The second-order analysis of stationary point processes," *Journal of Applied Probability*, vol. 13, no. 2, pp. 255–266, 1976.

[9] Thibault Lagache, Vannary Meas-Yedid, and Jean-Christophe Olivo-Marin, "A statistical analysis of spatial colocalization using ripley's k function," in *2013 IEEE 10th International Symposium on Biomedical Imaging*. IEEE, 2013, pp. 896–901.

[10] Thibault Lagache, Alexandre Grassart, Stéphane Dallongeville, Orestis Faklaris, Nathalie Sauvonnet, Alexandre Dufour, Lydia Danglot, and Jean-Christophe Olivo-Marin, "Mapping molecular assemblies with fluorescence microscopy and object-based spatial statistics," *Nature Communications*, vol. 9, no. 1, pp. 698, Dec. 2018.

[11] David L Donoho and Iain M Johnstone, "Ideal spatial adaptation by wavelet shrinkage," *Biometrika*, vol. 81, no. 3, pp. 425–455, 09 1994.

[12] Suvadip Mukherjee, Thibault Lagache, and Jean-Christophe Olivo-Marin, "Evaluating the stability of spatial keypoints via cluster core correspondence index," *IEEE Transactions on Image Processing*, vol. 30, pp. 386–401, 11 2020.

[13] Jesús Pérez-Ortega, Tzitzitlini Alejandre-García, and Rafael Yuste, "Long-term stability of neuronal ensembles in mouse visual cortex," *bioRxiv*, 2020.

[14] Samuel Kubler, Suvadip Mukherjee, Jean-Christophe Olivo-Marin, and Thibault Lagache, "A robust and versatile framework to compare spike detection methods in calcium imaging of neuronal activity," 04 2021, pp. 375–379.

[15] Eftychios A. Pnevmatikakis, Daniel Soudry, Yuanjun Gao, Timothy A. Machado, Josh Merel, David Pfau, Thomas Reardon, Yu Mu, Clay Lacefield, Weijian Yang, Misha Ahrens, Randy Bruno, Thomas M. Jessell, Darcy S. Peterka, Rafael Yuste, and Liam Paninski, "Simultaneous Denoising, Deconvolution, and Demixing of Calcium Imaging Data," *Neuron*, vol. 89, no. 2, pp. 285–299, Jan. 2016.

[16] Vincent D Blondel, Jean-Loup Guillaume, Renaud Lambiotte, and Etienne Lefebvre, "Fast unfolding of communities in large networks," *Journal of Statistical Mechanics: Theory and Experiment*, vol. 2008, no. 10, pp. P10008, Oct 2008.